

# Manipulating Electronic Energy Disorder in Colloidal Quantum Dot Solids for Enhanced Charge Carrier Transport

Sangjin Lee, David Zhitomirsky, and Jeffrey C. Grossman\*

A realistic CQD solid model is developed that computes the charge carrier mobility using hopping transport models within an ensemble of individual CQD units. Large decreases in electron mobility of up to 70% as compared to the monodisperse case are observed when the energetic disorder in CQD films lies in the typical experimental range of 10%–15%. Furthermore, it is suggested that tailored and potentially experimentally achievable re-arrangement of the CQD size ensemble combined with spatial doping control can mediate the reduction in mobility even in highly dispersive cases, and presents an avenue toward improved mobility and photovoltaic performance by up to 9% by leveraging fast carrier transport channels in highly polydisperse materials.

## 1. Introduction

Colloidal quantum dots (CQDs) have gained considerable attention<sup>[1–3]</sup> due to their unique optical and electronic properties that can be tuned by both size control and ligand engineering, leading to the use of CQD for optical devices, such as light emitting diodes,<sup>[4–7]</sup> photo detectors,<sup>[8–10]</sup> and solar cells.<sup>[11–17]</sup> However, such applications are limited by the relatively small charge carrier mobility ( $0.001\text{--}0.1\text{ cm}^2\text{ V}^{-1}\text{ s}^{-1}$ )<sup>[8,14,18]</sup> in CQD active layers, originating from the fact that the charge carrier transport depends mainly on slow kinetics: namely, a hopping transport mechanism.<sup>[19,20]</sup> A number of studies have explored ways to enhance the carrier mobility in CQD layers, including the use of shorter ligands,<sup>[21]</sup> reduction of trap density by surface passivation,<sup>[22,23]</sup> alignment of energy levels with ligands for nearly resonant transport,<sup>[24]</sup> and induction of band-like transport;<sup>[25]</sup> in some cases charge carrier mobilities higher than  $10\text{ cm}^2\text{ V}^{-1}\text{ s}^{-1}$  have been achieved.<sup>[26–29]</sup> Size dispersion in as-synthesized CQDs is considered another source of mobility loss and device performance degradation. CQDs synthesized from conventional wet-chemistry processes possess a 5%–15% size dispersion,<sup>[21,30,31]</sup> causing a corresponding dispersion in the energy gaps between the highest occupied molecular

orbital (HOMO) and the lowest unoccupied molecular orbital (LUMO) of the individual CQDs. This inhomogeneity in electronic energy levels can disrupt the charge hopping transport in CQD films and degrade the transport rate significantly. In addition, a sufficiently narrow CQD size dispersion is essential to achieve the periodic supercrystals that have shown dramatic enhancement in carrier mobility in CQD field effect transistors due to the reduced interparticle spacing and increased exchange coupling from the ligand treatments.<sup>[32]</sup> The impact of CQD size dispersion on the charge carrier mobility in CQD films

is little understood, and apparently contradictory results such as a lack of correlation between polydispersity and carrier mobility<sup>[21,33]</sup> versus the high carrier mobility observed using monodisperse CQDs,<sup>[32]</sup> calls for further investigation into the impact of radius distribution of CQDs on the carrier mobility in CQD films. Furthermore, while recent work showed that CQD solar cell performance was not influenced by polydispersity since a high density of deep trap states degraded the charge transport in CQD active layers regardless of their size dispersion,<sup>[34]</sup> new concepts involving small ionic ligands and hybrid passivation strategies could successfully inactivate those trap states,<sup>[23]</sup> motivating the need for detailed studies on the impact of the CQD polydispersity, and for the establishment of design rules for polydisperse CQD layers.

In this paper, we analyze the impact of the electronic energy disorder originating from the size dispersion of CQDs on the charge carrier mobility in CQD films under a hopping transport regime using computational approaches, in which we determine the equilibrium in the charge continuity equations for each CQD by taking into account all the possible hopping transport pairs within a given cut-off distance. We show how the manipulation of CQD size dispersion can effectively control the carrier mobility in CQD films. In particular, our results confirm that both the energy barriers and the diffusion barriers work simultaneously, blocking the charge carrier transfer in the case that a gradient exists in the radius profile along the electric field direction. We suggest that well-controlled doping helps circumvent the mobility drops from these coexisting barriers, and then show that forming networks of large CQDs through radius rearrangement in the direction perpendicular to the electric field promotes fast charge hopping transport efficiently.

S. Lee, Dr. D. Zhitomirsky, Prof. J. C. Grossman  
Massachusetts Institute of Technology  
77 Massachusetts Ave., Cambridge, MA 02139, USA  
E-mail: jcg@mit.edu



DOI: 10.1002/adfm.201504816

## 2. Result and Discussion

We prepared CQD films with size dispersions using molecular dynamics (MD) simulations, mimicking the experimental CQD film deposition process as described in the Section S1 in the Supporting Information; an example of the CQD film unit cell is given in Figure 1(a). Equilibrium positions were then used for estimating the charge transport performance of each CQD film. Our hopping transport simulations solve for the equilibrium for all CQDs in the charge continuity equations:

$$\frac{dN}{dt} = -U_{\text{net}} + R_{e,\text{in}} - R_{e,\text{out}} \quad (1)$$

$$\frac{dP}{dt} = -U_{\text{net}} + R_{h,\text{in}} - R_{h,\text{out}} \quad (2)$$

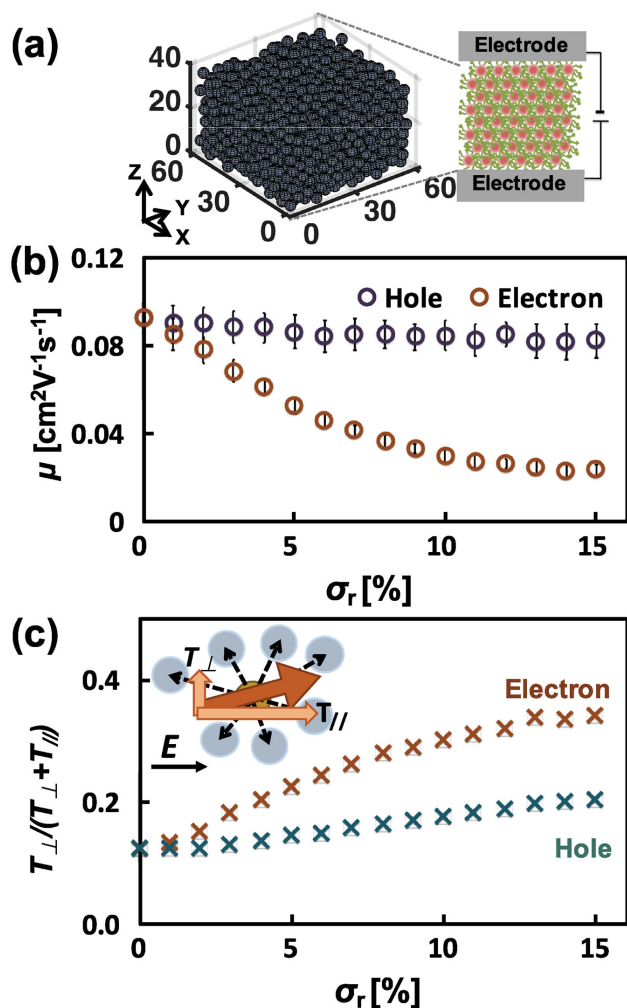


**Figure 1.** a) An example of CQD film unit cell for hopping transport simulation (left); two electrodes are set at the top and bottom of the unit cell (right). Electric fields are applied in the +z-direction. b) Charge carrier mobility of CQD films with respect to the polydispersity. c) The portions of charge transport rate perpendicular to the electric field increase as size dispersion increases.

where  $N(P)$  is the number of electrons (holes) in each CQD,  $U_{\text{net}}$  is the net recombination rate,  $R_{e,\text{in}}(R_{h,\text{in}})$  is the incoming rate of electrons (holes) from nearby CQDs within a predefined cut-off distance, and  $R_{e,\text{out}}(R_{h,\text{out}})$  is the outgoing rate of electrons (holes) into the nearby CQDs within the same predefined cut-off distance; charge transport complies with the variable-range hopping (VRH) mechanism,<sup>[35,36]</sup> where transport is not limited to the nearest hopping sites, especially for the highly disordered cases. Periodic boundary conditions are employed for the  $x$ - and  $y$ -directions. Each QD-to-QD charge transport rate was defined based on the Miller–Abraham hopping transport model:<sup>[37]</sup>

$$r_{d \rightarrow a} = N_d V_a H_f \exp\left(-\frac{d}{\alpha_d} - \frac{d}{\alpha_a} - \frac{\Delta E_{d \rightarrow a} + |\Delta E_{d \rightarrow a}|}{2kT}\right) \quad (3)$$

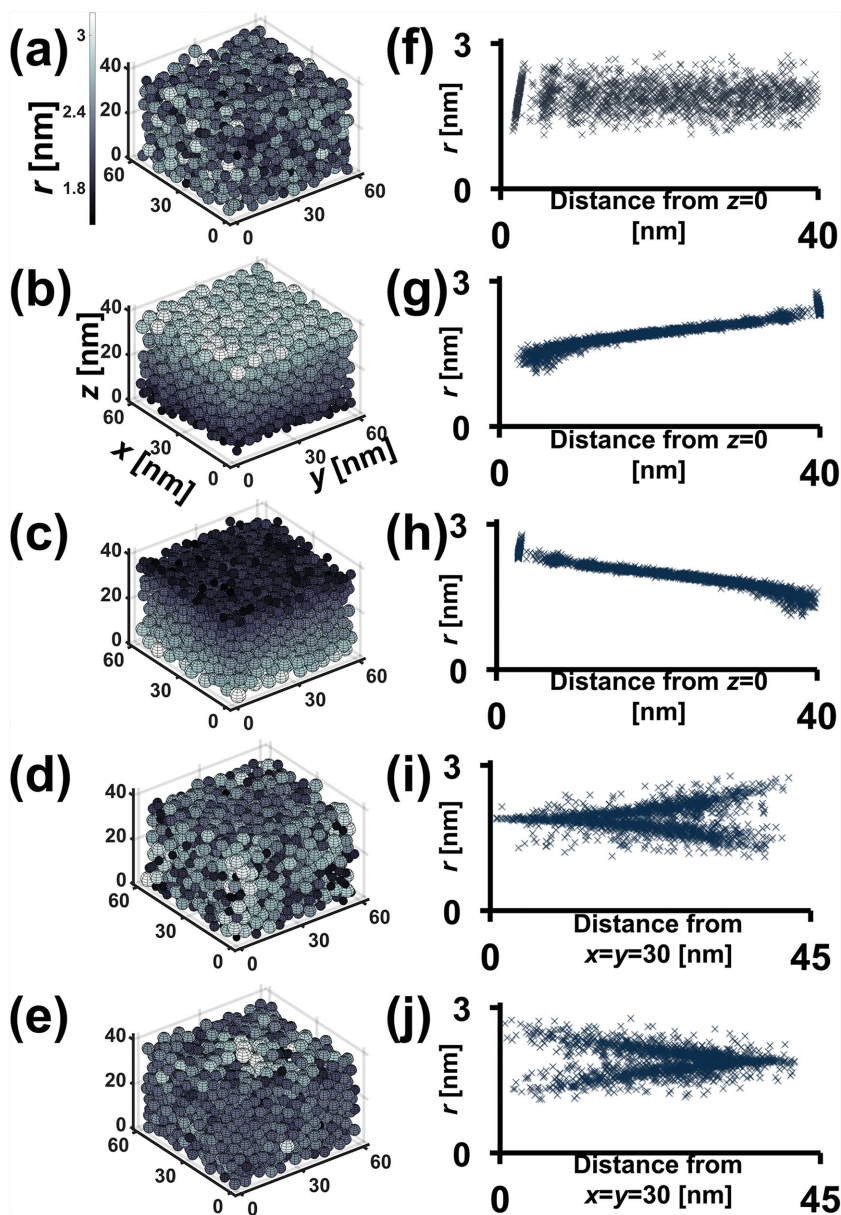
where  $r_{d \rightarrow a}$  is the hopping transport rate from a donor to an acceptor,  $H_f$  is the hopping frequency,  $N_d$  is the number of charges in the donor CQD,  $V_a$  is the ratio of empty states for the charge in the acceptor CQD,  $\alpha_d$  and  $\alpha_a$  represent the localization lengths of donor and acceptor CQDs, respectively, which is set to be comparable to their radii,<sup>[36]</sup>  $d$  is the distance between acceptor and donor CQDs, and  $\Delta E_{d \rightarrow a}$  is the energy difference when the charge transports from the donor to the acceptor. While the localization lengths can vary between CQDs, these changes can be absorbed into the hopping frequency coefficient,  $H_f$ , because we assume no enhancement or degradation of interactions in specific CQD pairs, or CQD ligands exists. This model implies that the charges need thermal activation in order to tunnel through the distance  $d$  from lower energy levels to higher energy levels. We note that variables in Equation (3) are time-averaged in the equilibrium of the charge continuity equations (Equations (1) and (2)); for example,  $N_d$  is allowed to be a non-integer. Although non-integer numbers for charges can significantly underestimate the Efros–Shklovskii VRH (ES-VRH) at low temperature, ES-VRH is known not to be dominant in the temperature used in our simulations (300 K).<sup>[38]</sup> Further details regarding our computational approach and code validation are given in the Sections S2 and S3 in the Supporting Information.

Figure 1(b) shows the trends of electron and hole mobility with increasing CQD size dispersion. 50 different samples were averaged for each size dispersion. Note that a 70% loss in the electron mobility is observed for samples of around 10% size dispersion, the typical standard deviation in CQD sizes in films prepared using conventional wet processes.<sup>[30]</sup> On the other hand, the hole mobility shows only a  $\approx 11\%$  decrease even in the most dispersive (15%) CQD radius distribution cases. This mobility reduction and the differences in electron and hole mobilities can be understood from the relation between spreads in site energy differences and the CQD size dispersion. Figure S5 in the Supporting Information shows the increases in the standard deviations in neighboring site energy differences ( $\Delta E$  when charge transport occurs between nearest hopping pairs) for all CQDs as the size dispersion broadens. Since the hopping transport Equation (3) includes the energy difference terms inside the exponent, the variance in the neighboring site energy differences diversifies the charge hopping transports into neighboring CQDs in terms of their directions and rates.

The smaller reduction in the hole mobility can also be attributed to the small increases in site energy deviation even for a large CQD size dispersion. We further tested this model to ensure accurate behavior given additional temperature and mean size parameters; more than 54% of electron mobility drops were observed from a wide variety of samples, the details of which are provided in the Section S6 in the Supporting Information.

In order to further analyze the impact of these divergences in hopping transport, we adopted *hopping rate vectors* that represent the intensity and directions of each charge hopping transport rate between all the transport pairs. Adding all the hopping rate vectors for the hopping transport pairs of each CQD, we obtained the overall transport rate and direction through each CQD, then evaluated how much of this transport rate differs from the electric field direction; we defined  $T_{\parallel}$  (parallel to the electric field) and  $T_{\perp}$  (perpendicular to the electric field) as shown in the inset in Figure 1(c) (see the Section S5 in the Supporting Information for further details).

The trends of  $T_{\perp}/(T_{\perp}+T_{\parallel})$  shown in Figure 1(c) imply that charge carrier mobility in CQD films degrades with increased size dispersion due to the inhomogeneity in energy level differences between hopping transport pairs which in turn alters the charge transport from the electric field direction, indicating that a larger portion of hopping transport rates in the electric field direction boosts the overall charge carrier mobility. This analysis of the mobility drops in polydisperse CQD films suggests that a reduction in the site energy deviations and an increase in electric-field-oriented charge transfer will serve as desirable design rules for higher mobility CQD films. One strategy to maintain the highest charge mobility in CQD films could involve synthesizing monodisperse CQDs or narrowing the size dispersion from the as-synthesized polydisperse CQDs before depositing as active layers. Achieving perfectly monodisperse CQDs is currently unrealistic given the hot-injection methods used in CQD synthesis and lack of efficient nanometer scale filtration methods, although recent work reported a 5% size dispersion;<sup>[39]</sup> however, even in this case our calculations show that 40% of the potential electron mobility is lost due to the size dispersion. Furthermore, several types of CQD systems including III–V composites inherently have difficulties in being prepared with small size dispersion<sup>[40]</sup> due to their unique synthesis process.<sup>[41]</sup> Another approach to achieve efficient charge transport in CQD films could be to redesign the CQD configurations within the film even though considerable size dispersion exists in the as-synthesized colloidal CQDs. While computational

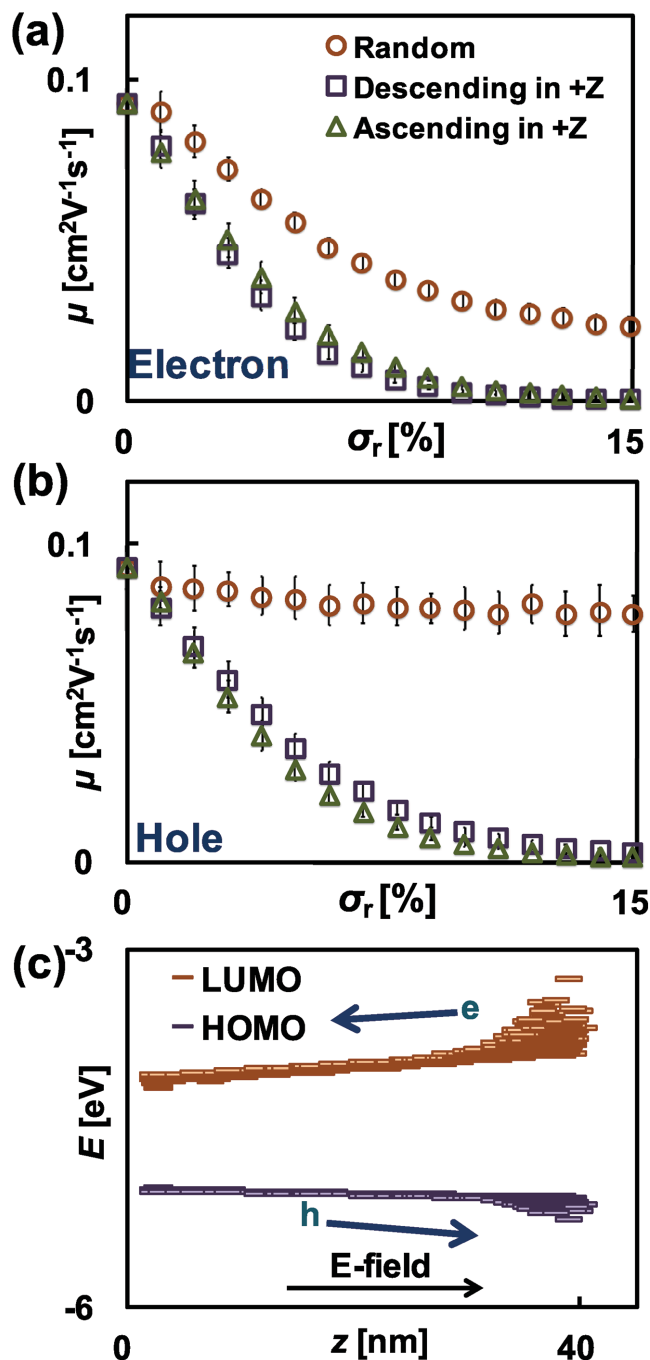


**Figure 2.** Examples of unit cells and radius distributions for the rearranging strategies used in this paper: a,f) random distribution, b,g) ascending radius in +z-direction, c,h) descending radius in +z-direction, d,i) increasing polydispersity as the distance from center increases, and e,j) decreasing polydispersity as the distance from center increased.

approaches allow for any distribution of CQDs to be tested, here we adopt ones that may be practically realized, such as a film possessing a gradient of colloidal CQD radii in different directions: vertical (in the electric field) or horizontal (perpendicular to the electric field). We prepared five different types of computational unit cells (Figure 2) where the effective radii of CQDs have: (1) a random distribution, (2) an ascending order in the +z-direction, (3) a descending order in the +z-direction, (4) an ascending order in size dispersion as a function of distance from the center, and (5) a descending order in size dispersion as a function of distance from the center. Examples of radius profiles for CQD locations in each unit cell are also

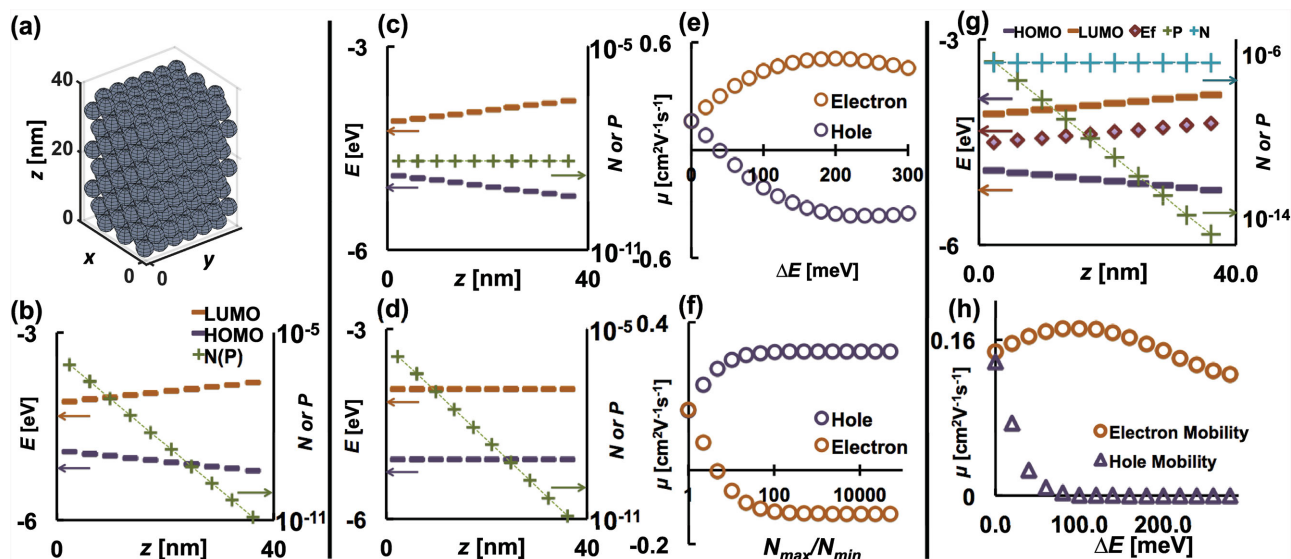
shown in Figure 2(f–j). While samples (2) and (3) have a gradient in the radii of CQDs, size dispersions rather than radii were controlled in the horizontal directions for samples (4) and (5); for example, sample (4) possesses a nearly monodisperse region near the center part of the simulation unit cell. The arrangements of CQD radii described above were applied prior to placing the CQDs into the simulation box and starting the MD simulation since artifacts such as unphysical overlapping of neighboring CQDs are possibly introduced into the CQD geometry if the positions of CQDs are exchanged after the MD equilibration. In addition, this pre-deposition sorting guarantees that all five types of radii distributions and size-dispersion gradient controls are generated from the same initial CQD radius distribution for each size dispersion from 0% to 15%.

Figure 3(a,b) shows the dramatic reductions in charge carrier mobility as the size dispersion increases, for both electrons and holes. Contrary to the case of random samples, the CQD films with the descending (ascending) radius gradient impose continuous energy barriers for charge hopping; in the case of descending (ascending) radius gradient, holes (electrons) need extra thermal energy to overcome these energy barriers, which leads to large drops in the charge carrier mobility. Surprisingly, the mobility for opposite charge (electrons for descending radius-gradient samples and holes for ascending radius-gradient samples) shows a large decrease, which is not intuitive from the electric energy diagram shown in Figure 3(c). Electrons (holes) can travel without energy barriers toward the electrode on the left (right) side via CQD networks along a downhill network of energy levels. Equation (3) implies that charges hopping from higher energy levels to lower energy levels do not need thermal activation. Therefore, the mobility of the opposite charges should show limited drops or even an improvement for the oriented size dispersion, as opposed to the results we find in Figure 3(a,b). In order to elucidate the source of these large and counter-intuitive drops in mobility for both electrons and holes, we prepared a simpler CQD simulation sample with a face-centered-cubic-like (FCC-like) configuration as shown in Figure 4(a). When the HOMO–LUMO gaps possess a gradient in the  $z$ -direction as in the descending case, the number of charges that show exponential increases along the HOMO–LUMO gap decrease because more electrons can be thermally excited from HOMO to LUMO levels in the case of the smaller energy gaps (see Figure 4(b)). Next we separate the impact of energy barrier and diffusion barrier by forcing the limit on each of them. Figure 4(c) shows the case where we keep the number of charges constant regardless of HOMO–LUMO gaps. Under positive bias in the  $+z$ -direction, electrons travel in the  $-z$ -direction without experiencing energy barriers while holes should overcome the thermal energy barriers when they hop toward the electrode near  $z = 40$ . This contrast in transport behaviors results in complete opposite trends in electron and hole mobility as shown in Figure 4(e); as the gradient in HOMO–LUMO gap increases, the hole mobility drops significantly even to negative values, which indicates the positive charges tend to move in the opposite direction of the electric field. In Figure 4(d), we show results with constant HOMO–LUMO gaps with exponentially increasing number of charges as the  $z$ -position of the CQDs approaches the bias electrode at  $z = 0$ . Although there is no energy barrier for both electrons



**Figure 3.** a,b) Charge carrier mobility with respect to CQD size dispersion when CQD sizes have ascending and descending order in  $+z$ -directions; dramatic reductions in mobility are observed for both electrons and holes. The energy diagram for a descending case (c) indicates that holes should overcome the energy barrier while electrons travel downhill of energy levels with an electric field in the  $+z$ -direction.

and holes in this case under the positive electric field in the  $+z$ -direction, Figure 4(f) indicates that the electron mobility drops severely when the  $N_{\max}$ -to- $N_{\min}$  ratio increases, where  $N_{\max}$  ( $N_{\min}$ ) is the maximum (minimum) number of charges in a single CQD in the simulation unit cell. Since Equation (3) implies that a donor CQD with larger charge population allows



**Figure 4.** Analysis of energy and diffusion barriers with simpler CQD simulation sample; a) a unit cell of the face-centered-cubic CQD configuration and b) distribution of electronic energy levels when sizes of CQDs are sorted along the electric field direction (+z). When the number of equilibrium charges is forced to be constant c) with the same energy level distribution with (b), the energy barriers solely work for hole transport (e). In the case of constant HOMO–LUMO gaps d) with the same number of equilibrium charges with (b), diffusion barriers work for electrons that travel in –z-direction (f), where  $N_{\max}/N_{\min}$  indicates the maximum (minimum) number of equilibrium charges in the CQD films. g) Control of the doping profile can circumvent those coexisting energy and diffusion barriers, h) making mobility for one type of charge (electron for this example) stay high even for a large gradient in the energy levels.

higher transport rates, more charge numbers near the bias electrode promotes such a large electron transfer in the +z-direction that the electron mobility can turn negative when the gradient in the number of charges is extremely steep. In other words, electrons have to overcome the diffusion barrier from the larger number of electrons in the CQDs “ahead” in the traveling direction. Thus, the significant decreases in charge carrier mobility for both electrons and holes in the case of descending and ascending radius distributions can be attributed to the fact that diffusion barriers as well as energy barriers serve to simultaneously block transport of all charge carriers. While CQDs with smaller HOMO–LUMO gaps can provide downhill energy pathways that lead to easy charge transport free from energy barriers, a larger number of charges in those smaller gap CQDs will, in turn, prevent those carriers from moving freely through the downward energy gradient. These results suggest that the charge distribution in CQD films should be carefully taken into account when designing CQD-based optoelectronic devices where a variety of strategies, including quantum funnels<sup>[42]</sup> and tandem structures,<sup>[12,43]</sup> are applied to enhance the device performance. Circumventing these coexisting charge transport barriers inevitably requires another method to separate the number of charges and the HOMO–LUMO gap. Figure 4(g,h) shows that an elaborate doping of CQDs would remove the diffusion barrier effectively. Here, we used FCC-like CQD films where the Fermi levels were set parallel to the LUMO levels by corresponding doping as shown in Figure 4(g). Note that the first CQD layers near the bias electrode at  $z = 0$  were p-doped for the sake of unblocked electron transfer in the –z-direction, leading to the invariable electron mobility even for CQD films where high gradients exist in energy levels along the electric field (Figure 4(h)). However, not only would such a strategy

require sophisticated additional processes for doping profile control, but it cannot provide fast charge transfer for both electrons and holes simultaneously because the doping profiles induce an imbalance between both electrodes and accumulate a built-in electric field in the –z-direction for the case of Figure 4(g), leading to increased energy barriers for holes to travel toward the electrode at  $z = 0$ . These drawbacks, in turn, call for alternative ways to improve mobility other than CQD radius rearrangement along the electric field direction; in particular, we next explore the potential of horizontal sorting of CQD radii to suppress  $T_{\perp}/(T_{\perp}+T_{\parallel})$ .

The trends in carrier mobility for the case where the size dispersion is sorted in horizontal directions are shown in Figure 5(a,b). Interestingly, the electron mobility shows a smaller drop than the unsorted random cases, bounded at about 40% even when the colloidal CQD films have large size dispersions, which indicates that these types of size-dispersion controls may be useful strategies to ease the mobility drop in polydisperse CQD layers. The redesign of size dispersion in horizontal directions leads to the development of two channels through which the charge carriers move faster than the random cases: smaller disperse paths (Figure 5(d), upper) where charge transport stays in the electric field direction as explained earlier, and networks of large CQDs (Figure 5(e), lower) where lower site energy differences between larger CQDs bring about higher carrier mobility.<sup>[21]</sup> We confirmed that the latter transport paths actually play effective roles in the mobility enhancement using a simulation cell with ‘tail’ CQDs that have smaller or larger radii than 1-sigma value of the normal distribution. The inset in Figure 5(b) shows an example of the radii distribution used. The trends in charge carrier mobility for these tail samples are in good agreement with both cases of horizontal rearrangement

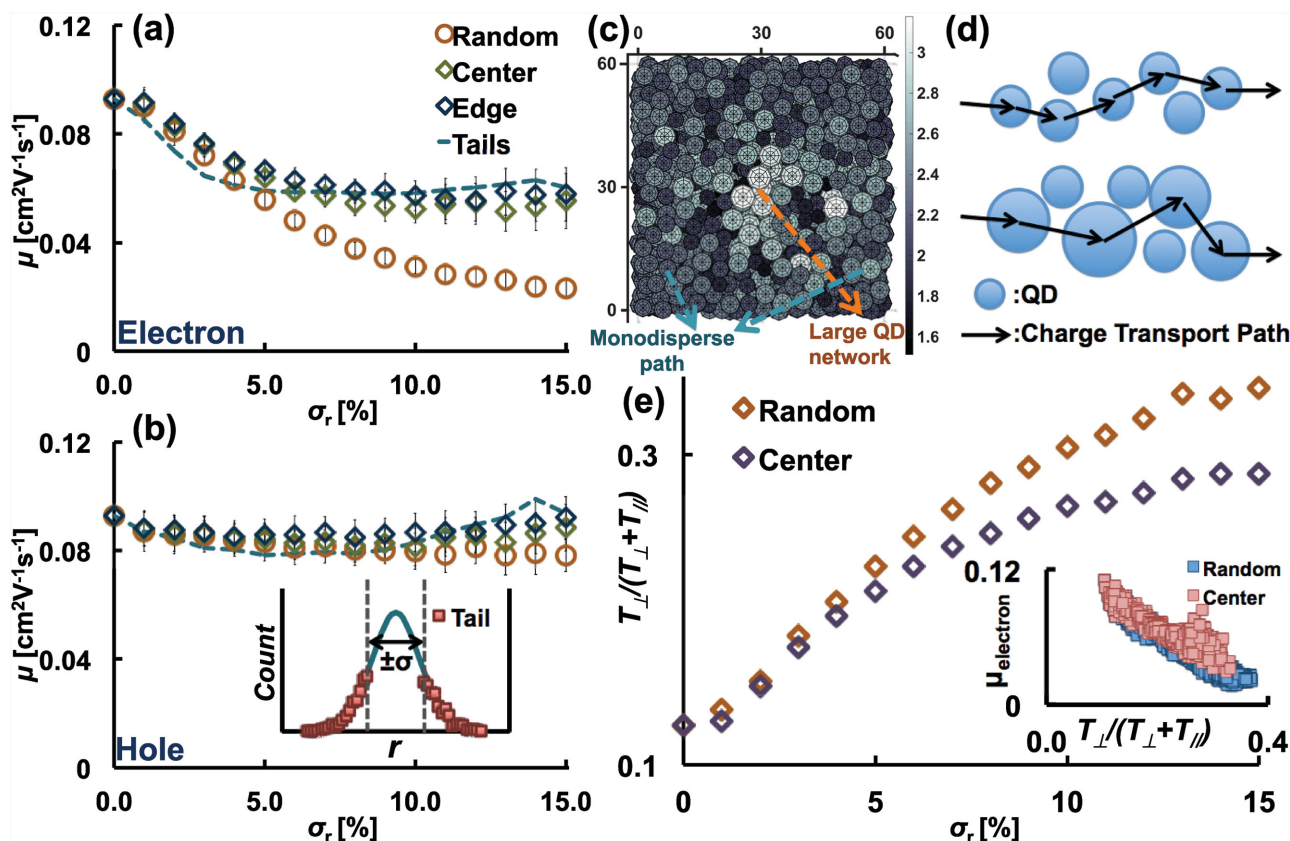


**Figure 5.** Charge carrier mobility for a) electrons and b) holes with respect to the CQD size dispersion when CQD films have the size-dispersion gradients in horizontal directions; center (edge) indicates the samples with smaller size dispersion in the center (edge) of the unit cell; and tails indicates the samples with smaller or larger size QDs than 1-sigma value of the normal distribution as shown in the inset. c) Possible paths for higher charge carrier mobility than random cases. d) Illustrations of charge hopping transports for small-dispersion path (upper) and the network of large QDs (bottom). e) The network of large QDs promotes the charge transfer along the electric field direction, where comparison in trends of transport rate portions not in the electric field direction between random and center samples is given.

of CQD size dispersions. Hopping rate vector analysis confirms that networks of large QDs played a role in maintaining the lower  $T_{\perp}/(T_{\perp}+T_{\parallel})$  even at higher size dispersion than that in the randomly arranged CQD films as shown in Figure 5(e).

Limiting the mobility drops up to 40% with the networks of large QDs in polydisperse CQD films, compared to the  $\approx 70\%$  drops in random cases, provides straightforward improvement in the CQD device performance. For example, the higher mobility would enhance the photovoltaic performance of CQD films, allowing more charge extraction and thicker light-absorbing layers. In order to ascertain the impact of spatially tailoring a CQD film to take advantage of the size dispersion, we developed a fully self-consistent optoelectronic device simulator that used our CQD simulation boxes as inputs. **Figure 6(a)** shows the computed  $J$ - $V$  curves for the random and the horizontally sorted CQD films with external charge generation. While polydispersity in CQD films largely degrades all of the photovoltaic performance parameters (8% in short-circuit current, 15% in open-circuit voltage, 16% in the fill factor, and 34% in power conversion efficiency at 10% polydispersity), with a major impact on open circuit voltage as known from experimental literature,<sup>[34]</sup> the CQD films with the networks of large QDs, fitted with dashed line in Figure 6(a), facilitate

efficient charge extractions; 7% and 9% improved PCEs were estimated for 10% and 15% polydisperse samples, respectively. Importantly, the percolation networks affect only the current and do not negatively impact the device open circuit voltage. Interestingly, percolation networks using intragap states have recently been reported to be able to sustain appreciable currents within a CQD solid.<sup>[44]</sup> Furthermore, the enhancements in charge extraction increase when thicker CQD films are used as shown in Figure 6(b), indicating that more useful light absorption is available with the improved carrier mobility. The doubled charge carrier mobility expected from the networks of large QDs with  $\approx 10\%$  size dispersion enables a roughly 40% enhancement in diffusion length and possible CQD film thickness, leading to a 17% enhanced device performance predicted from the optoelectronic modeling based on experimental data.<sup>[45]</sup>

Our results suggest that further experimental work toward realizing such design strategies could lead to large improvements in device performance. Despite the successful achievements of well-designed CQD film structures with size gradients<sup>[42]</sup> or graded dopings,<sup>[46]</sup> the films were deposited using multistep spin-coating processes. In order to apply a CQD radius gradient along the electric field with controlled doping,

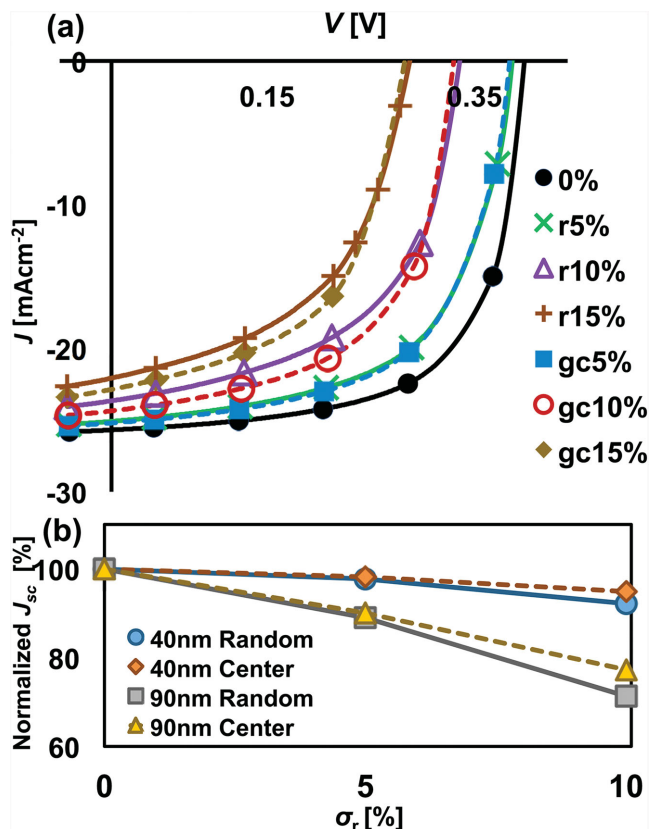


**Figure 6.** a) Photovoltaic performance of CQD films; numbers in the indices mean the polydispersity (%) and “r” (“gc”) indicates sample with random arrangements (gradient in size dispersion with smaller dispersion in center), and b) trends in the short-circuit currents, normalized by the value from monodisperse CQD films.

a new technique combining existing doping controls (mainly from ligand exchanges) and simultaneous size sorting (i.e., centrifuging<sup>[47]</sup>) is needed. On the other hand, the horizontal size-dispersion controls for the networks of large CQDs cannot be achieved without novel methods for separating CQDs with specific sizes. Optical sorting techniques<sup>[48–50]</sup> can work for this since they change the distribution of nanoparticles with respect to their sizes possibly even during the deposition processes; however, further improvements are necessary due to the extremely small size of CQDs and significant solvent flows during the spin-coating. Combination with slower CQD deposition processes such as electrophoresis,<sup>[51]</sup> Langmuir–Blodgett technique<sup>[52]</sup> or Langmuir–Schaefer technique<sup>[53]</sup> can provide scopes for the development of favorable sorting methods.

### 3. Conclusion

In conclusion, using a combination of computational procedures including MD simulations and hopping transport calculations, we have examined the impact of polydispersity on carrier mobility in colloidal CQD solids. Our results show that the carrier mobility of colloidal CQD layers depends strongly on the distribution of the individual CQD’s size. Engineering the HOMO–LUMO gaps, therefore, needs sophisticated

consideration in order not to block the charge carrier transport through both energy barriers and diffusion barriers. We have proposed doping strategies to circumvent these coexisting diffusion barriers, and our results suggest that the redesign of size distributions could also enable fast carrier transport by introducing networks of large CQDs. Importantly, this approach could result in high mobilities even in the case of highly polydisperse colloidal CQD films. While photovoltaic performances of CQD films were largely degraded by random size dispersion, our newly introduced concept of networks of large CQDs promoted efficient charge extraction with device performance improvements as high as 9% in power conversion efficiency. This highlights that there is tremendous opportunity to improve performance either by isolating perfectly monodisperse nanocrystals, or, engineering deposition strategies to form high-mobility percolation networks that may be suitable for a variety of CQD optoelectronic devices.

### 4. Computational Section

**Charge Carrier Mobility:** Computational samples of CQD films with 0%–15% size dispersions were prepared using MD simulations in the LAMMPS package.<sup>[54]</sup> Assuming each CQD with 4 Å ligand length is a sphere, 1600 radii of CQDs were generated with a normal distribution with standard deviation ranging from 0 to 0.285 nm and an average radius of 1.9 nm. We refer to the bottom of the simulation cell as the  $xy$ -plane (60 nm × 60 nm) located at  $z = 0$  and the height of the cell corresponds to the  $z$ -axis (Figure 1(a)). After the CQD spheres are sparsely placed above the simulation box, the MD simulation starts with an additional acceleration in  $-z$ -direction, which causes the CQDs to drop into the simulation box where periodic boundary conditions in the  $x$ - and  $y$ -directions area applied. The CQD spheres find their equilibrium positions under a granular potential that defines interactions among CQDs; a strong repulsive force acts only when the distance between two CQD spheres becomes less than the sum of their radii. Generated CQD films from these procedures have randomly close-packed configurations with packing density around 0.605, in good agreement with the reported results on the trend of core to total volume ratio with respect to the inter-CQD distance in the face-centered-cubic-like amorphous phase;<sup>[55]</sup> an example CQD configuration is shown in Figure 1. Next, positions and radii of CQDs were used to model transport where HOMO–LUMO gaps were calculated using a relation for lead sulfide (PbS) CQDs suggested by Moreels et al.<sup>[56]</sup> While the HOMO–LUMO gap broadens as the CQD size decreases due to the quantum confinement effect, the changes in the individual energy levels are not symmetric. We therefore determined the HOMO and LUMO levels based directly on experimental results from Hyun et al.<sup>[57]</sup> In this model we assumed that charges hop via HOMO or LUMO levels, but note that additional effects such as charging energy and polaronic effects may be implemented to increase its accuracy, though they would dramatically increase model complexity and computation time (see the Section S4 in the Supporting Information for the details).

The electrodes were set on either side of the CQD film (top and bottom as shown in Figure 1(a)) and their work functions

were set to the equilibrium points where the net charge transfer between each electrode and the CQD film became zero. The mobility of CQD films was estimated using the current density at 0.001 V nm<sup>-1</sup> electric field, comparable to the electric field inside the depletion layer in conventional CQD solar cells working at the maximum power point<sup>[45]</sup> or that between sources and drains in CQD field effect transistors,<sup>[25]</sup> and the total number of carriers in the layers when all the charge continuity Equations (1) and (2) became close enough to zero so that the current densities converged to within 10<sup>-8</sup> of the relative tolerance. In addition to these charge continuity equations, Poisson equations defined the electric potentials of all CQDs. The multivariable Newton's method was applied to find this equilibrium; details can be found in the Section S2 in the Supporting Information. We also show the applicability of our modeling platform across other materials systems by simulating commonly reported NaZn13 structures,<sup>[58,59]</sup> with details in the Section S7 in the Supporting Information.

**Photovoltaic Performances:** We used the same CQD film unit cells as shown in Figure 2 for photovoltaic performance estimation. CQDs are p-doped with 10<sup>-4</sup> positive charge per each CQD, leading to Fermi levels at about 0.3 eV above the HOMO levels. Hole blocking boundary conditions replaced the ohmic ground electrode at the maximum z coordinate of the unit cells; this boundary condition serves as hole blocking layers in heterojunction CQD solar cells. Optical generation terms are added into the right sides of Equations (1) and (2). A constant value of 4 × 10<sup>3</sup> was used for those generation rates for all CQDs.

## Supporting Information

Supporting Information is available from the Wiley Online Library or from the author.

## Acknowledgements

This work was supported by the Samsung Advanced Institute of Technology and the computations in this research used resources of the National Energy Research Scientific Computing Center, a DOE Office of Science User Facility supported by the Office of Science of the U.S. Department of Energy under Contract No. DE-AC02-05CH11231.

Received: November 10, 2015

Revised: December 10, 2015

Published online:

- [1] C. R. Kagan, C. B. Murray, M. Nirmal, M. G. Bawendi, *Phys. Rev. Lett.* **1996**, *76*, 1517.
- [2] C. B. Murray, C. R. Kagan, M. G. Bawendi, *Science* **1995**, *270*, 1335.
- [3] C. B. Murray, D. J. Norns, M. G. Bawendi, *J. Am. Chem. Soc.* **1993**, *115*, 8706.
- [4] V. L. Colvin, M. C. Schlamp, A. P. Alivisatos, *Nature* **1994**, *370*, 354.
- [5] B. O. Dabbousi, M. G. Bawendi, O. Onitsuka, M. F. Rubner, *Appl. Phys. Lett.* **1995**, *66*, 1316.
- [6] K. Cho, E. K. Lee, W. Joo, E. Jang, T. Kim, S. J. Lee, S. Kwon, J. Y. Han, B. Kim, B. L. Choi, J. M. Kim, *Nat. Photonics* **2009**, *3*, 341.
- [7] B. S. Mashford, M. Stevenson, Z. Popovic, C. Hamilton, Z. Zhou, C. Breen, J. Steckel, V. Bulovic, M. Bawendi, S. Coe-Sullivan, P. T. Kazlas, *Nat. Photonics* **2013**, *7*, 407.
- [8] J. P. Clifford, G. Konstantatos, K. W. Johnston, S. Hoogland, L. Levina, E. H. Sargent, *Nat. Nanotechnol.* **2009**, *4*, 40.
- [9] G. Konstantatos, I. Howard, A. Fischer, S. Hoogland, J. Clifford, E. Klem, L. Levina, E. H. Sargent, *Nature* **2006**, *442*, 180.
- [10] S. a. McDonald, G. Konstantatos, S. Zhang, P. W. Cyr, E. J. D. Klem, L. Levina, E. H. Sargent, *Nat. Mater.* **2005**, *4*, 138.
- [11] J. Tang, E. H. Sargent, *Adv. Mater.* **2011**, *23*, 12.
- [12] X. Wang, G. Koleilat, J. Tang, H. Liu, *Nat. Photonics* **2011**, *5*, 480.
- [13] G. H. Carey, K. W. Chou, B. Yan, A. R. Kirmani, A. Amassian, E. H. Sargent, *MRS Commun.* **2013**, *3*, 83.
- [14] J. Tang, K. W. Kemp, S. Hoogland, K. S. Jeong, H. Liu, L. Levina, M. Furukawa, X. Wang, R. Debnath, D. Cha, K. W. Chou, A. Fischer, A. Amassian, J. B. Asbury, E. H. Sargent, *Nat. Mater.* **2011**, *10*, 765.
- [15] J. J. Choi, Y.-F. Lim, M. B. Santiago-Berrios, M. Oh, B.-R. Hyun, L. Sun, A. C. Bartnik, A. Goedhart, G. G. Malliaras, H. D. Abruña, F. W. Wise, T. Hanrath, *Nano Lett.* **2009**, *9*, 3749.
- [16] K. W. Johnston, A. G. Pattantyus-Abraham, J. P. Clifford, S. H. Myrskog, D. D. MacNeil, L. Levina, E. H. Sargent, *Appl. Phys. Lett.* **2008**, *92*, 151115.
- [17] C.-H. M. Chuang, P. R. Brown, V. Bulović, M. G. Bawendi, *Nat. Mater.* **2014**, *13*, 796.
- [18] K. W. Johnston, A. G. Pattantyus-Abraham, J. P. Clifford, S. H. Myrskog, S. Hoogland, H. Shukla, E. J. D. Klem, L. Levina, E. H. Sargent, *Appl. Phys. Lett.* **2008**, *92*, 122111.
- [19] P. Guyot-Sionnest, *J. Phys. Chem. Lett.* **2012**, *3*, 1169.
- [20] I.-H. Chu, M. Radulaski, N. Vukmirovic, H.-P. Cheng, L.-W. Wang, *J. Phys. Chem. C* **2011**, *115*, 21409.
- [21] Y. Liu, M. Gibbs, J. Puthussery, S. Gaik, R. Ihly, H. W. Hillhouse, M. Law, *Nano Lett.* **2010**, *10*, 1960.
- [22] D. Zhitomirsky, M. Furukawa, J. Tang, P. Stadler, S. Hoogland, O. Voznyy, H. Liu, E. H. Sargent, *Adv. Mater.* **2012**, *24*, 6181.
- [23] A. H. Ip, S. M. Thon, S. Hoogland, O. Voznyy, D. Zhitomirsky, R. Debnath, L. Levina, L. R. Rollny, G. H. Carey, A. Fischer, K. W. Kemp, I. J. Kramer, Z. Ning, A. J. Labelle, K. W. Chou, A. Amassian, E. H. Sargent, *Nat. Nanotechnol.* **2012**, *7*, 577.
- [24] M. Scheele, D. Hanifi, D. Zhrebetsky, S. T. Chourou, S. Axnanda, B. J. Rancatore, K. Thorkelsson, T. Xu, Z. Liu, L. Wang, Y. Liu, a. P. Alivisatos, *ACS Nano* **2014**, *3*, 2532.
- [25] J.-S. Lee, M. V. Kovalenko, J. Huang, D. S. Chung, D. V. Talapin, *Nat. Nanotechnol.* **2011**, *6*, 348.
- [26] J.-H. Choi, A. T. Fafarman, S. J. Oh, D.-K. Ko, D. K. Kim, B. T. Diroll, S. Muramoto, J. G. Gillen, C. B. Murray, C. R. Kagan, *Nano Lett.* **2012**, *12*, 2631.
- [27] S. J. Oh, N. E. Berry, J.-H. Choi, E. A. Gaubling, T. Paik, S.-H. Hong, C. B. Murray, C. R. Kagan, *ACS Nano* **2013**, *7*, 2413.
- [28] W. Liu, J. Lee, D. V. Talapin, *J. Am. Chem. Soc.* **2013**, *135*, 1349.
- [29] H. Zhang, J. Jang, W. Liu, D. V. Talapin, *ACS Nano* **2014**, *8*, 7359.
- [30] K. Bian, Z. Wang, T. Hanrath, *J. Am. Chem. Soc.* **2012**, *134*, 10787.
- [31] J. Yang, T. Ling, W.-T. Wu, H. Liu, M.-R. Gao, C. Ling, L. Li, X.-W. Du, *Nat. Commun.* **2013**, *4*, 1695.
- [32] D. V. Talapin, C. B. Murray, *Science* **2005**, *310*, 86.
- [33] H. Lepage, A. Kaminski-cachopo, A. Poncet, G. Carval, M. Campus, G. Cedex, I. Lyon, J. Capelle, *J. Phys. Chem. C* **2012**, *116*, 10873.
- [34] D. Zhitomirsky, I. J. Kramer, A. J. Labelle, A. Fischer, R. Debnath, J. Pan, O. M. Bakr, E. H. Sargent, *Nano Lett.* **2012**, *12*, 1007.
- [35] N. F. Mott, *J. Non Cryst. Solids* **1968**, *1*, 1.
- [36] D. Yu, C. Wang, B. L. Wehrenberg, P. Guyot-Sionnest, *Phys. Rev. Lett.* **2004**, *92*, 216802.
- [37] A. Miller, E. Abrahams, *Phys. Rev.* **1960**, *120*, 745.
- [38] M. S. Kang, A. Sahu, D. J. Norris, C. D. Frisbie, *Nano Lett.* **2011**, *11*, 3887.

- [39] M. C. Weidman, M. E. Beck, R. S. Hoffman, F. Prins, W. A. Tisdale, *ACS Nano* **2014**, *8*, 6363.
- [40] M. J. Anc, N. L. Pickett, N. C. Gresty, J. a. Harris, K. C. Mishra, *ECS J. Solid State Sci. Technol.* **2012**, *2*, R3071.
- [41] P. M. Allen, B. J. Walker, M. G. Bawendi, *Angew. Chem. Int. Ed.* **2010**, *49*, 760.
- [42] I. Kramer, L. Levina, R. Debnath, *Nano Lett.* **2011**, *11*, 3701.
- [43] P. K. Santra, P. V. Kamat, *J. Am. Chem. Soc.* **2013**, *135*, 877.
- [44] Y. Zhang, D. Zherebetsky, N. D. Bronstein, S. Barja, L. Lichtenstein, D. Schuppisser, L.-W. Wang, a. P. Alivisatos, M. Salmeron, *Nano Lett.* **2015**, *15*, 3249.
- [45] D. Zhitomirsky, O. Voznyy, L. Levina, S. Hoogland, K. W. Kemp, A. H. Ip, S. M. Thon, E. H. Sargent, *Nat. Commun.* **2014**, *5*, 3803.
- [46] Z. Ning, D. Zhitomirsky, V. Adinolfi, B. Sutherland, J. Xu, O. Voznyy, P. Maraghechi, X. Lan, S. Hoogland, Y. Ren, E. H. Sargent, *Adv. Mater.* **2013**, *25*, 1719.
- [47] J. Y. Kim, V. Adinolfi, B. R. Sutherland, O. Voznyy, S. J. Kwon, T. W. Kim, J. Kim, H. Ihee, K. Kemp, M. Adachi, M. Yuan, I. Kramer, D. Zhitomirsky, S. Hoogland, E. H. Sargent, *Nat. Commun.* **2015**, *6*, 7772.
- [48] P. Ják, T. Čížmár, M. Šerý, P. Zemánek, *Appl. Phys. Lett.* **2008**, *92*, 2013.
- [49] I. Ricárdez-Vargas, P. Rodríguez-Montero, R. Ramos-García, K. Volke-Sepúlveda, *Appl. Phys. Lett.* **2006**, *88*, 121116.
- [50] T. Čížmár, M. Šiler, M. Šerý, P. Zemánek, V. Garcés-Chávez, K. Dholakia, *Phys. Rev. B—Condens. Matter Mater. Phys.* **2006**, *74*, 035105.
- [51] K. W. Song, R. Costi, *Adv. Mater.* **2013**, *25*, 1420.
- [52] A. Gole, N. R. Jana, S. T. Selvan, J. Y. Ying, *Langmuir* **2008**, *24*, 8181.
- [53] K. Lambert, R. K. Čapek, M. I. Bodnarchuk, M. V. Kovalenko, D. Van Thourhout, W. Heiss, Z. Hens, *Langmuir* **2010**, *26*, 7732.
- [54] S. Plimpton, *J. Comput. Phys.* **1995**, *117*, 1.
- [55] Z. Wang, C. Schliehe, K. Bian, D. Dale, W. a. Bassett, T. Hanrath, C. Klinke, H. Weller, *Nano Lett.* **2013**, *13*, 1303.
- [56] I. Moreels, K. Lambert, D. Smeets, D. De Muynck, T. Nolle, J. C. Martins, F. Vanhaecke, A. Vantomme, C. Delerue, G. Allan, Z. Hens, *ACS Nano* **2009**, *3*, 3023.
- [57] B. Hyun, Y. Zhong, A. C. Bartnik, L. Sun, H. D. Abrun, F. W. Wise, J. D. Goodreau, J. R. Matthews, T. M. Leslie, N. F. Borrelli, *ACS Nano* **2008**, *2*, 2206.
- [58] E. V. Shevchenko, D. V. Talapin, N. a Kotov, S. O'Brien, C. B. Murray, *Nature* **2006**, *439*, 55.
- [59] E. V. Shevchenko, D. V. Talapin, S. O'brien, C. B. Murray, *J. Am. Chem. Soc.* **2005**, *127*, 8741.